UCRL-JC-124504
PREPRINT

Gain Saturation Studies in LG-750 and LG-770 Amplifier Glass

D. M. Pennington, D. Milam, and D. Eimerl

**This paper was prepared for submittal to
2nd Annual International Conference on Solid-State Lasers for Applications to Inertial Confinement Fusion
Paris, France
October 22-25, 1996**

March 10, 1997

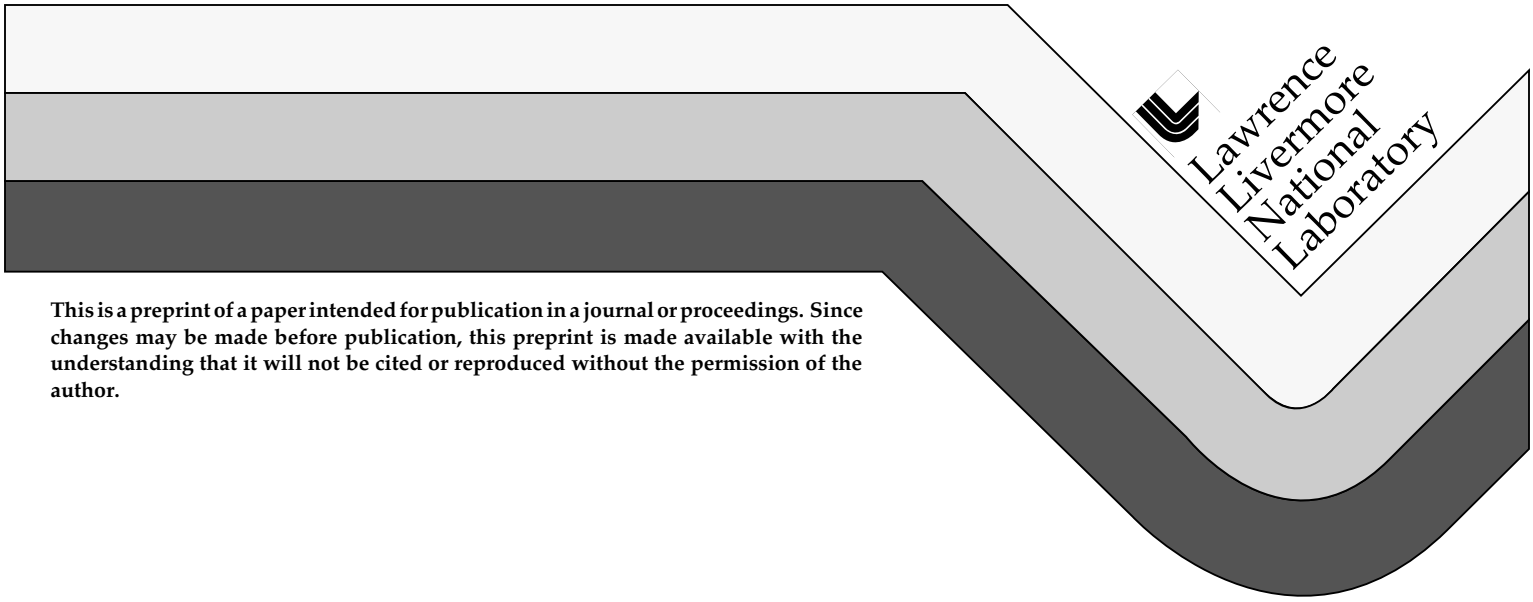

GAIN SATURATION STUDIES IN LG-750 AND LG-770 AMPLIFIER GLASS

D. M. Pennington, D. Milam, and D. Eimerl
Laser Program, Lawrence Livermore National Laboratory,
PO Box 808, L-439, Livermore, CA 94550

ABSTRACT

Experiments were performed on the 100-J class Optical Sciences Laser (OSL) at LLNL to characterize the saturation fluence and small-signal gain of a solid-state Nd:glass amplifier utilizing LG-750 and LG-770, an amplifier glass developed for the National Ignition Facility (NIF). These high quality measurements of gain saturation at NIF level fluences, i.e., 10-15 J/cm^2, provide essential parameters for the amplifier performance codes used to design NIF and future high power laser systems. The small-signal gain, saturation fluence and square-pulse distortion were measured as a function of input fluence and pulse length in platinum-free LG-750 and LG-770. The input fluence, output fluence, small-signal gain and passive losses were measured to allow calculation of the saturation fluence. Least squares fits of the output vs. input fluence data using a Frantz-Nodvik[1] model was used to obtain an average saturation fluence for each data set. Overall, gain saturation in LG-750 and LG-770 is comparable at long pulse lengths. For shorter pulse lengths, < 5 ns, LG-770 exhibits a stronger pulse length dependence than LG-750, possibly due to a longer terminal level lifetime. LG-770 also has a higher cross-section, which is reflected by its slightly higher extraction efficiency.

Keywords: gain saturation, small-signal gain, Nd:doped phosphate amplifier glass

1.0 INTRODUCTION

The characteristics of neodymium doped glasses under saturated gain conditions are important when calculating the energy parameters of amplifier systems and in determining the energy that can be extracted from an active medium.[2-6] Saturation of a glass amplifier is a function of the input fluence, the laser pulse shape and duration, wavelength, bandwidth, and polarization of the extracting beam, the relaxation rates in the laser glass, the operating temperature, etc.. All of these parameters affect the extraction efficiency, which in turn affect the laser cost. Accurate saturation models are essential for the amplification codes used to design NIF and future high power laser systems.

In a glass, the environment around each ion can differ due to local variations in the crystal field. This results in site-to-site differences in the energy levels and the radiative and nonradiative transition probabilities of the individual ions. The superposition of the individual states broadens the homogeneous linewidth of the glass. The fluorescence line width of a glass is a measure of the extent of the Stark splitting of the initial and final energy levels and inhomogeneous broadening resulting from the site-to-site variations in the crystal field. This width is determined by the glass network-forming and network-modifying ligands - the more uniform the coordination shell around the ion, the narrower the fluorescent line width. Performance of neodymium-doped glass amplifiers is complicated by the Stark splitting and inhomogeneous broadening of the levels of the $^4F_{3/2}$ to $^4I_{11/2}$ lasing transition[7-9], spectral migration of energy between excited centers[8-11], scatter of the stimulated transition cross sections for the Stark components of individual ions[8,9,12], dependence of the cross sections on the polarization of laser radiation[13-18], etc.

In the 1.06 μm Nd-doped glass lasing transition the active upper level $^4F_{3/2}$ is split into two Stark components and the lower level $^4I_{11/2}$ is split into six components, as shown in Fig. 1. The luminescence line of a Nd^{3+} ion consists of 12 superimposed spectral components with different intensity

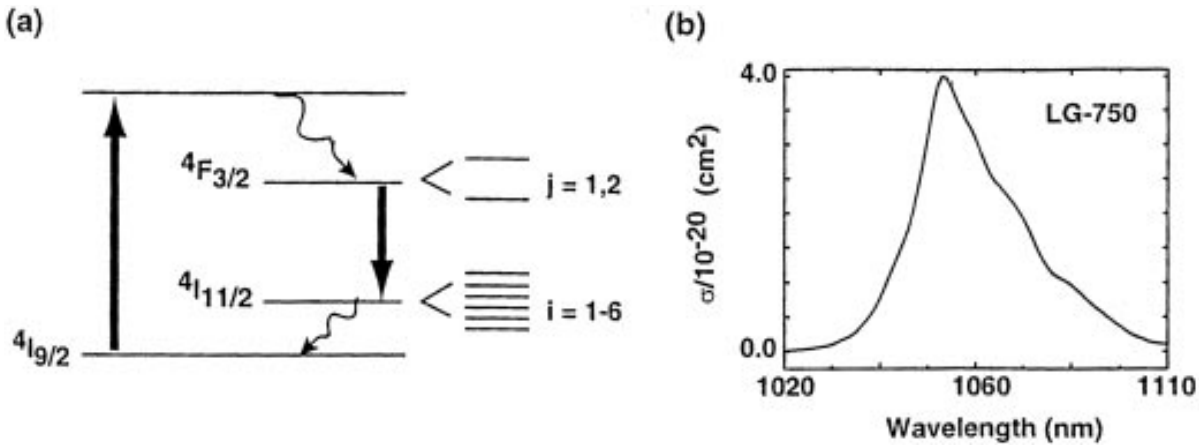

Fig. 1: (a) In the 1.06 mm Nd-doped glass lasing transition the active upper level $^4F_{3/2}$ is split into two Stark components and the lower level $^4I_{11/2}$ is split into six components. (b) The luminescence line of a Nd^{3+} ion consists of 12 superimposed spectral components with different intensity profiles, as shown for LG-750.

profiles, governed by a convolution of the Gaussian distribution function of excited centers with the Lorentzian distribution of the probability of transitions in individual ions. The Stark splitting of the $^4F_{3/2}$ and $^4I_{11/2}$ energy levels in LG-750 is approximately 114 cm^{-1} and 75 cm^{-1}, respectively, with an inhomogeneous line width of ~80 cm^{-1}.[19] Equilibration time between the Stark levels of a given ion is on the order of 1 ps, while the time required for cross-relaxation between Nd^{3+} ions in spectrally different sites ranges between 1ms and 1 ms depending on the glass.[20] Because of inhomogeneous broadening, the 12 transition levels between the two degenerate levels of the $^4F_{3/2}$ to the six levels of the $^4I_{11/2}$ state are not resolved, thus measurement of the stimulated emission cross section is limited to the integrated characteristics of the emission curve, shown in Fig. 1(b) for LG-750. Moreover, there is significant variation in the cross section values reported in the literature (2.0-4.8 x 10^{-20} cm^2 for phosphate glass).[7-10,13-15,21,22]. Consequently, simulation of the energy extraction for multitransition, inhomogeneously broadened lines is difficult and uncertain because the positions, widths, strengths, and correlations of the individual transitions are not accurately known.

Numerous experimental studies and modeling of gain saturation and extraction efficiency in Nd:glass are reported in the literature[1,4,13,16-20,23-45] The most relevant studies for our purposes are those of Martin and Milam[18,23,25] and Yarema and Milam[17,24], in which a thorough study was made of gain saturation in Nd-doped silicate, phosphate and fluorophosphate glasses as a function of fluence, wavelength, and pulse duration. Several important observations were made in these experiments. The measured saturation fluence showed a small but distinct pulse length dependence, attributed to the finite relaxation time of the terminal level. The saturation fluence was observed to increase as a function of input fluence. In general, the saturation fluence was found to be less than $h\nu/\sigma$, where ν is the frequency of the extracting radiation.

Calculations of the saturation fluence for the $^4F_{3/2}$ to $^4I_{11/2}$ transition are generally made using the Frantz-Nodvik equation, which takes the following form for a homogeneously broadened medium and a collimated beam in the absence of passive losses[1]:

$$E_{out} = E_{sat} \ln(1 + e^{g_o l}(e^{E_{in}/E_{sat}} - 1)) \quad , \qquad (1)$$

where E_{in} and E_{out} are the fluence at the input and output to the amplifier, respectively, g_o is the small signal gain, l is the length of the amplifying medium; $E_{sat} = h\nu/\sigma$, is the saturation fluence for a

homogeneous medium, where $h\nu$ is the photon energy and σ is the stimulated emission cross section. To account for absorption losses the Frantz-Nodvik equation can be written in the more general form[45]:

$$ln\, g_o = \int_{E_{in}}^{E_{out}} \frac{dE}{E_{sat}(1 - exp(E/E_{sat}) - \delta/\alpha_o} \quad . \tag{2}$$

Here a_o is the gain coefficient and δ is the loss coefficient computed by attributing passive loss to uniform bulk absorption and/or scattering. Over the past few years the narrowband saturation data taken by Martin and Milam[18,23,25] and Yarema and Milam[17,24] has been modeled extensively, using the Frantz-Nodvik equation, corrected numerically to account for passive losses[17,18,25,26]. This modeling demonstrates that in the saturated regime E_{sat} is not proportional to $h\nu/\sigma$, but to $kh\nu/\sigma$, where k is a correction factor that depends upon the glass type, or in a more fundamental sense, upon the degree of inhomogeneous broadening of the fluorescence line of the glass. The value of k can vary from 0.5 in LG-56 to 0.87 in LG-750.[18,23,25] This result can be interpreted as being due to a linear superposition of individual oscillators at various sites that do not all have the same homogeneous line width or line position. Thus the individual sites that have their peak cross section at the extracting wavelength will saturate relatively easily, while those for which the extracting wavelength lies in the wings of the line will exhibit a measurably higher saturation fluence due to the lower effective cross section at the extracting wavelength.

To describe the variation of the measured saturation fluence from Frantz-Nodvik predictions, a multiple ion model can be used.[18,28] Neodymium ions in a glass laser media reside in a variety of physical environments and experience different perturbing local fields. As a result, the stimulated emission cross section describing the interaction of an ion with an electromagnetic field of specified frequency and polarization also varies from site-to-site, and a distribution of cross sections are required to describe amplification. In its simplest form, the multiple ion model assumes that there are two kinds of ions in the glass, with cross section values σ_1 and σ_2, respectively, but the approach outlined below can be generalized to include an arbitrarily large number of cross sections as well. The population-weighted average cross section is required to be equal to the Judd-Ofelt cross section so that the small signal gain per unit of stored energy remains constant.[18,46] Thus $\sigma_{J\text{-}O} = F\sigma_1 + (1\text{-}F)\sigma_2$, where F is the fraction of ions with cross section σ_1. This gives rise to two saturation fluences:

$$E_{s1} = \frac{hc}{\sigma_1(1+K)\lambda} = E_s \frac{\sigma}{\sigma_1}$$

and (3)

$$E_{s2} = \frac{hc}{\sigma_2(1+K)\lambda} = E_s \frac{\sigma}{\sigma_2},$$

where K is a degeneracy factor, defined as a ratio of the degeneracies for the upper $^4F_{3/2}$ and lower $^4I_{11/2}$ Nd levels, and is presumed to be the same for both ions. The two-ion system is modeled by dividing the sample into spatial slices of gain much less than 1.1, applying the Frantz-Nodvik eqn. to calculate the gain calculation for each slice, taking losses at the input and output corresponding to any fixed losses, and then doing the amplification by the two ions one after the other. The extracting beam is propagated through a slice once to extract the first set of ions, giving the first saturation fluence. The beam is then propagated through a second time to extract the second set of ions, providing a second saturation fluence. The process is repeated until the entire medium has been extracted. The variables F, K, and σ_1 are varied to fit the experimental data. While this model does not provide one unique fit, it does fit the data with more accuracy than a single saturation fluence since the model phenomenologically accounts for variation of the saturation fluence with beam fluence.

The terminal level lifetime is also an important parameter in determining the extraction efficiency of a glass amplifier, as the magnitude of the pulse length relative to the lifetime determines whether the system operates as a three or four level laser. When the pulse length is comparable to the terminal level lifetime, the upward and downward transition rates at the laser frequency compete, thus the metastable population in the $^4I_{3/2}$ level becomes bottlenecked during extraction, and the laser approaches a three level operating condition. This effect also reduces the effective saturation fluence encountered by an extracting pulse in an amplifier. A phenomenological expression developed to describe the impact of the lower level lifetime on the saturation fluence in LG-750 is given by[47]:

$$E_{sat}(t_p, \tau_{11/2}) = \frac{E_o}{\{1+(\frac{g_u}{g_l})\exp(-t_p/\tau_{11/2})\}}\ , \qquad (4)$$

where E_o is the saturation fluence for a four level system, g_u is the upper level degeneracy, g_l is the lower level degeneracy, t_p is the pulse length, and $\tau_{11/2}$ is the terminal level lifetime. Bibeau, et.al., determined this lifetime to be on the order of 225 ps for most phosphate glasses.[48] Pulse duration and shape should have an effect on the extraction efficiency only if the pulse length approaches the 225 ps lifetime of the Nd^{3+} population in the $^4I_{11/2}$ level in the host laser glass. This is consistent with the numerous gain saturation measurements reported in the literature. More recently Bibeau, et. al. have developed an empirical formula for the saturation fluence that includes the ration of the pulse length, t_p, to the terminal level lifetime, $\tau_{11/2}$:[39]

$$F_{sat} = \frac{h\nu}{\sigma_{eff} * B(R)}, \text{where } B(R) = a_1\exp(-R/b_1) + a_2\exp(-R/b_2) + a_3\exp(-R/b_3)\,. \qquad (5)$$

Here $R = t_p/\tau_{11/2}$,$\sigma_{eff} = f_i\,\sigma_i$, where i = 1, 2 for the two-ion model, and a_i and b_i are parameters determined empirically from fitting experimental data.[39] This description accurately fits the Yarema-Milam data for LG-750, and should be applicable for other glasses with similar or better homogeneity.

2.0 EXPERIMENT

Experiments in the OSL were designed to characterize the saturation fluence and small-signal gain of a solid-state Nd:glass amplifier utilizing a proposed NIF amplifier glass, LG-770. The initial experiments were performed in platinum-free LG-750 to allow comparison of the results taken with the new experimental set-up with previous measurements[17]. This also provided the first off-line measurements of the saturation fluence at NIF level fluences, i.e., 10-15 J/cm^2. The experimental set-up used is shown in Fig. 2. The best-suited readily available amplifier chassis for these measurements holds a 2.5-cm diameter by 26-cm length rod with an active gain length of 20.3 cm. The rods were cut with parallel 6° wedges on each end to prevent internal reflections. Both ends of the rods were coated with high damage threshold AR coatings. The test rods were pumped by a six xenon flashlamps connected in series to a circuit with 50 μF and 300 μH. The resulting flashlamp pulse was 367 μsec in duration at the 10% point. This provided a gain of 15 at the peak of the curve. The gain was varied by shifting the timing of the extraction pulse relative to the peak with good reproducibility. The 1053-nm input beam was produced by a 100-ns Q-switched Nd:YLF oscillator. Different pulse lengths were sliced from the 100-ns envelope by a Pockels cell with a 100 ps rise and fall time. These were amplified to provide an input fluence of up to ~ 6 J/cm^2 at the input to the test amplifier. The beam was collimated to a 2-cm diam. to maximize extraction, while minimizing radial pump effects. Both LG-750 and LG-770 amplifier rods were cut from glass poured for amplifier slabs with ~ 2% Nd doping level. As a result, it was necessary to put a Gaussian crown on the input spatial beam profile in order to obtain a flat top spatial beam profile at the output of the experiment saturation amplifier. Representative input and output beam profiles are shown.

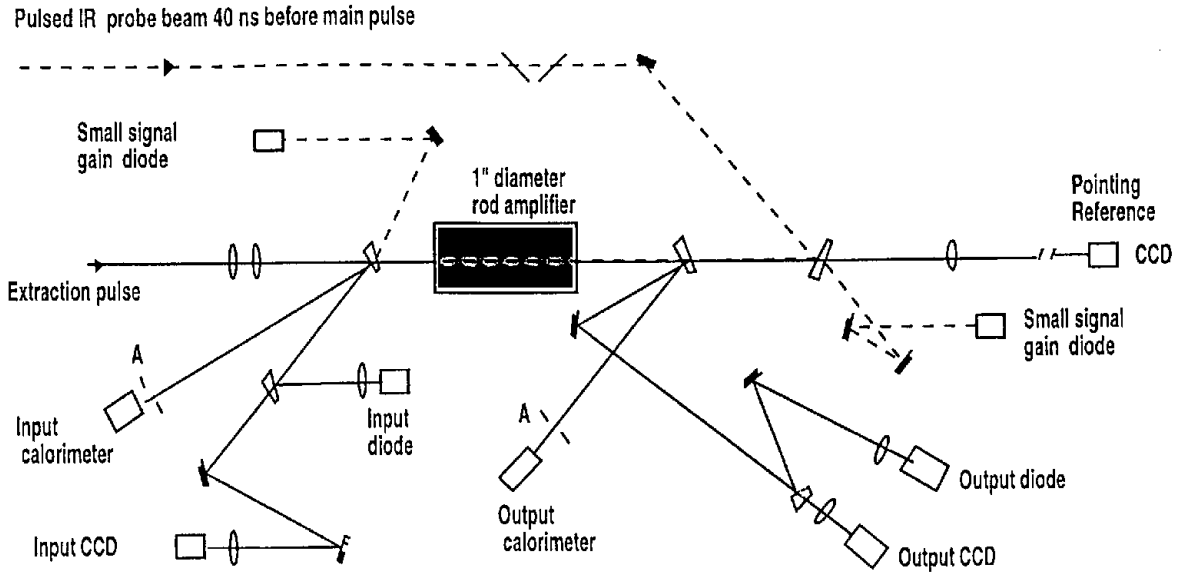

Fig. 2: The experimental set-up used to measure the saturated and small signal gain in an Nd:glass amplifier.

in Fig. 3. Since saturation is relatively insensitive to spatial beam modulations, an average fluence can be used to account for small spatial beam modulations.

The input fluence, output fluence, small-signal gain and passive losses were measured for each shot. Calorimetry was performed over the central 13 mm of the beam to eliminate regions of varying intensity in the skirt of the beam. This was accomplished by independently aperturing each beam before the Scientec 38-0111 calorimeters, being careful to sample the same region of the beam in both cases. The calorimeters were fed by paths that contained only bare fused silica wedges, and a *p*-polarized beam was used so the percent of each pulse that arrived at each calorimeter could be accurately calculated from measurements of the incident angles. The spatially averaged fluence in the diagnostic beams was calculated as the ratio of the transmitted energy to the area of the aperture. The aperture diameters were measured by an optical comparator to ± 0.15%. Fluences in the diagnostic beam were related to the fluences in the main beam through the Fresnel coefficients of the bare fused silica splitters that provided the diagnostic beams. The combined error on each fluence, including the aperture size, Fresnel reflectivity, calorimeter, signal amplifier and Labview recording system was 1% per fluence for calorimeter energies 20 mJ and 2% for energies < 20 mJ. The pulse shape was recorded before and after amplification via fast photodiodes and SCD5000 oscilloscopes with a resolution of approximately 3 GHz bandwidth. Fast photodiode traces provided a record of temporal pulse distortion due to gain saturation. Beam profiles were recorded at the input and output of the amplifier by Cohu 4800 CCD cameras for each shot.

The rod transmission was measured by three independent means. First the rod transmission was measured off-line in the Nova photometry facility. In the second method, the *in situ* rod transmission was measured using the experimental set-up shown in Fig. 4. A mirror was placed at the input of the test amplifier and the incident beam was retro-reflected back on itself. The light reflected off the bare surface splitter in each direction into integrating diodes. The mirror was then moved after the test amplifier, and the signals were measured. The ratio of the signals provided a measure of the double-pass passive loss in the rod. A third measure of the passive loss was obtained periodically by measuring the ratio of the transmitted main beam fluence to the incident main fluence without firing the saturation amplifier. The

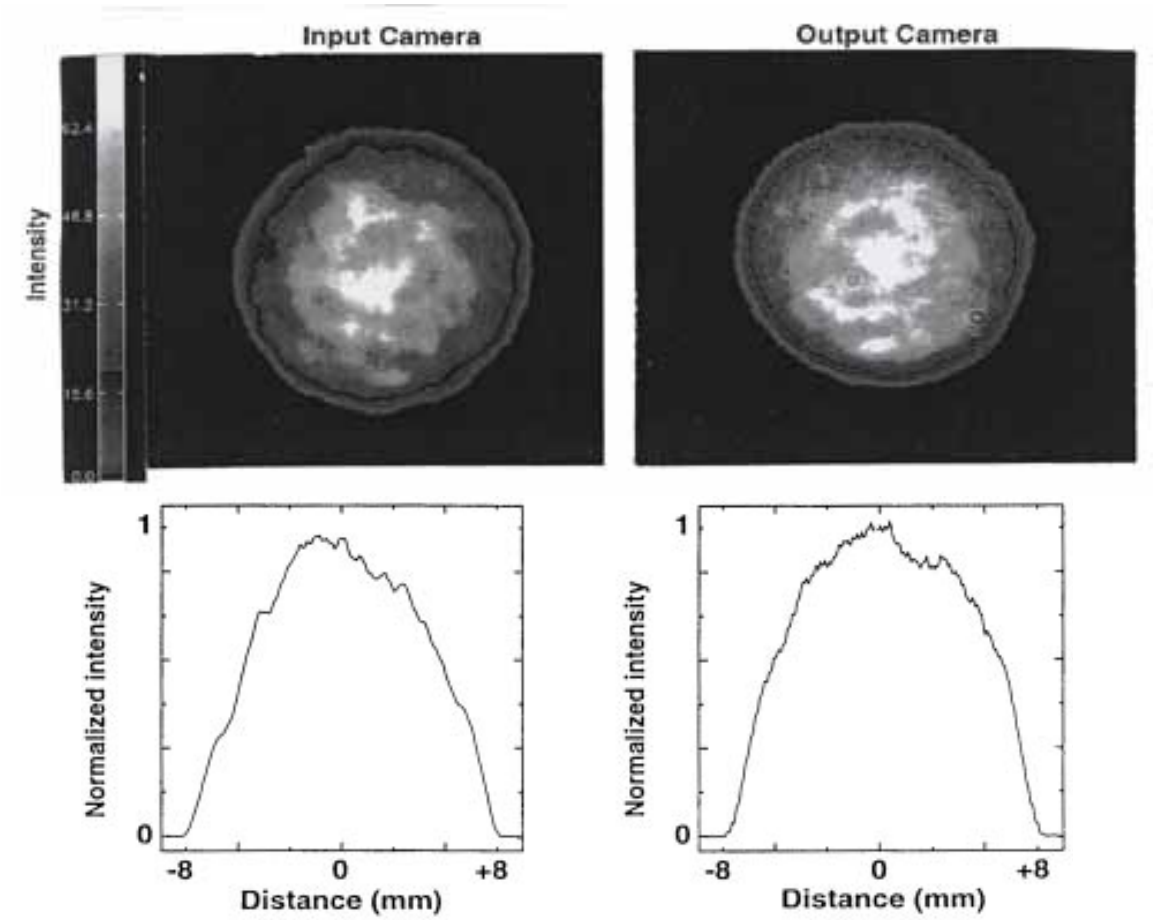

Fig. 3: Representative beam profiles taken at the input and output of the saturation test amplifier.

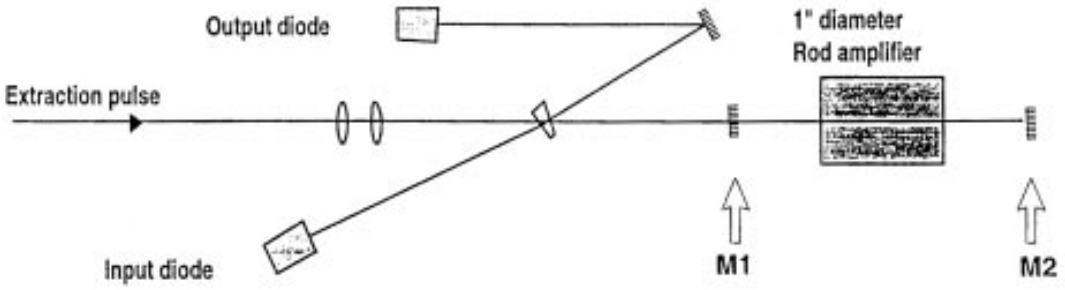

Fig. 4: Experimental set-up used to measure the *in situ* rod transmission. The ratio of signals from the output and input diodes was meeasured with a high reflector at locations M1 and M2

transmission obtained by each of these methods, the associated standard deviation, and the mean transmission and standard deviation of the mean for each glass are given in Table 1. The mean transmission and standard deviation of the mean were calculated using standard statistical techniques.[49]

TABLE 1	% Transmission (method 1)	% Transmission (method 2)	% Transmission (method 3)	Average % Transmission
LG-750	N/A	96.5, σ = 1.2	95.6, σ = 1.3	96.2, σ = 0.13
LG-770	97.6 , σ = 0.12	96.5 , σ = 0.37	97.3, σ = 0.45	97.5 , σ = 0.11

To measure the small-signal gain on each shot, a percentage of the pulse was split off early in the OSL amplifier chain, and was delivered to the experiment table 40 ns before the arrival of the main extraction pulse. The probe beam pulse length was the same as the extraction pulse. Probe energy was adjusted to be in the small signal gain regime, with ~ 10 mJ of energy for the 17 ns pulse length. The probe beam was *s*-polarized, and inserted into the saturation amplifier by reflection off the bare fused silica output diagnostic splitter, as shown in Fig. 2. The use of *s*-polarization provided isolation of the probe beam from the rest of the *p*-polarized laser chain, and was experimentally verified to have no effect on the small-signal gain measurement. The input energy of the probe beam was measured via an integrating photodiode looking at the light transmitted through the injection splitter. The reflected probe beam propagated through the saturation amplifier in the opposite direction of the extraction pulse. The small-signal gain probe beam was also 13 mm in diameter, and probed the same spatial region of the rod as sampled by calorimetry. The amplified probe beam energy was measured by a second integrating photodiode. Data was taken for each input fluence with and without firing the test amplifier to obtain the small-signal gain. The background was also obtained on each shot by monitoring the diode voltage before the arrival of the pulse, providing a background normalization. The ratio of the two measurements with and without the amplifier provided a means of obtaining a background-free small-signal gain measurement unobtainable in previous cw measurements.[17,18,25] This technique resulted in a small-signal gain measurement with an error of less than 0.5%.

3.0 DATA AND MODELING

Measurements of the small-signal gain and saturation fluence were made at 1053 nm in LG-750 for 1, 13, and 17-ns pulse lengths and in LG-770 for 1, 5, and 17-ns pulse lengths, with fluences up to 15 J/cm^2 at the longest pulse length. The results for LG-750 are in good agreement with previously reported results[17] which ended at ~10 J/cm^2. They also provide the first careful measurement of the saturation fluence as a function of output fluence at NIF level fluences, i.e., 10-15 J/cm^2. Modeling of each data set used the following experimentally determined cross section values, σLG-750 = 3.6 x 10^{-20} cm^2 and σLG-77o = 3.9 x 10^{-20} cm^2.[50]

3.1 LG-750

Results of the 17-ns pulse length experiments in LG-750 are shown in Fig. 5. The data shows the expected linear increase in saturation fluence as a function of output. The Yarema-Milam data[17], plotted along with the current LG-750 data in Fig. 5(b), is consistent with the OSL results. The data can be fit to simple linear function, $F_{sat} = a\,F_{out} + b$, where the slope a = 0.08, and the intercept b = 3.77 J/cm^2.

Each data set was fit using both the single-ion and two-ion Frantz-Nodvik models. Since the terminal level lifetime is on the order of 225 ps in LG-750[48], the 20-ns Milam Yarema data should be experimentally indistinguishable from 17-ns OSL data. The best fit to the Milam Yarema data using the single-ion model for a 20 ns pulse length is obtained using an average saturation fluence value of 4.52 J/cm^2, assuming a cross-section of 3.6 x 10^{-20} cm^2. This saturation fluence also fits the current data set for output fluences 10 J/cm^2. The results of the single-ion model are shown in Fig 6 for the OSL 17-ns data. Note that as the fluence increases beyond 10 J/cm^2, the model deviates from the data. To accurately model the high fluence data points (>10 J/cm^2), a saturation fluence of 4.71 J/cm^2 is required. This data is consistent with gain measurements taken on Beamlet[51] at high fluence.

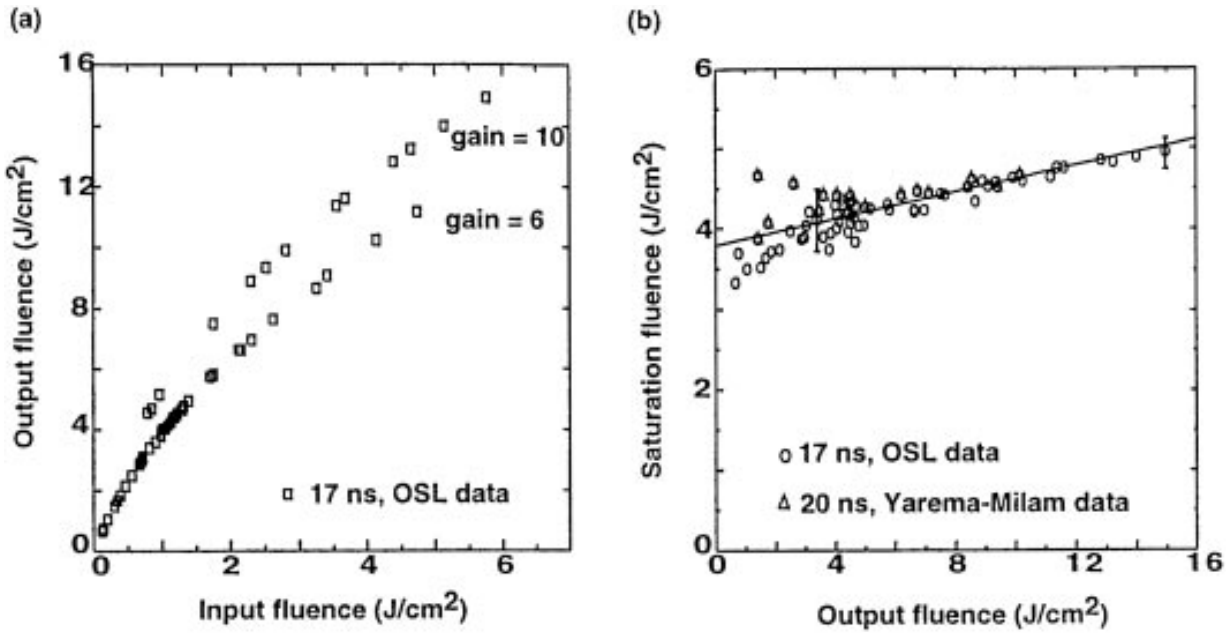

Fig. 5: Results of the 17-ns pulse length OSL and 20 ns Yarema-Milam experiments in LG-750 are plotted. (a) The plot of fluence out vs fluence in shows good agreement between the current experiment and previous results. Part (b) shows the saturation fluence increases linearly with output fluence.

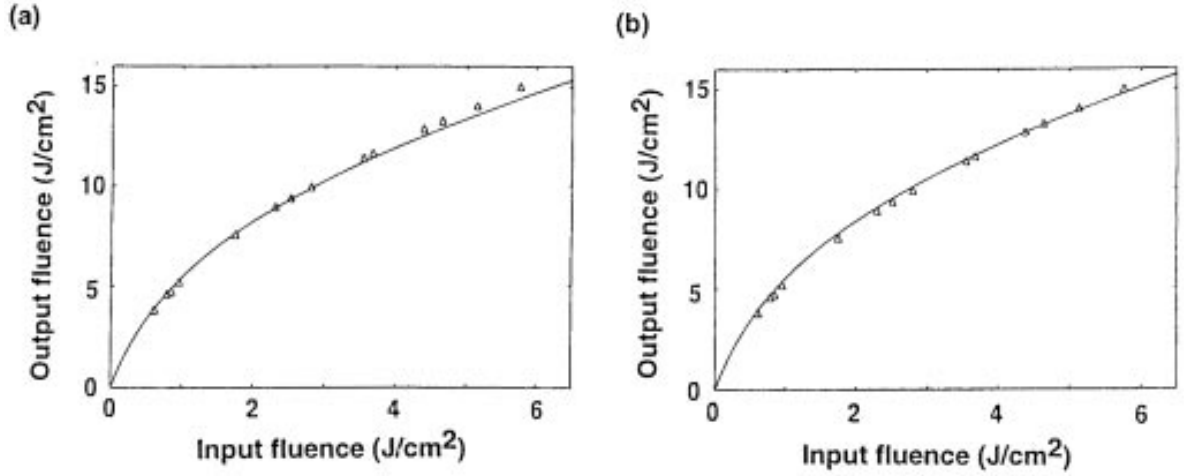

Fig. 6: The results of a single-ion model analysis are shown for the OSL 17-ns data. Different saturation fluence values are needed to fit the data at low and high output fluence using a single-ion model. (a) The low fluence data is fit best by F_{sat} = 4.52 J/cm^2, assuming σ = 4.17 x 10^{-20} cm^2, while (b) the high fluence data is best fit by F_{sat} = 4.71 J/cm^2, assuming σ = 4.01 x 10^{-20} cm^2.

We have also modeled the data using the two-ion model. Using this method, a locus of fits can be obtained that accurately fit the data. To narrow in on the best fit, a least square optimization routine was used to minimize the standard deviation. Modeling was performed for the high-fluence OSL data, low-fluence OSL data and the Yarema-Milam data. All three data sets can be fit with similar parameters. The best fit to the current OSL data set, with $\sigma_{residual}$ = 0.03 J/cm^2, is shown in Fig. 7. In each case, one ion type makes up approximately 82% of the population with a saturation fluence of ~ 2.40 J/cm^2. The remaining 18% of the population is in the second fraction, with a saturation fluence of ~ 7.87 J/cm^2.

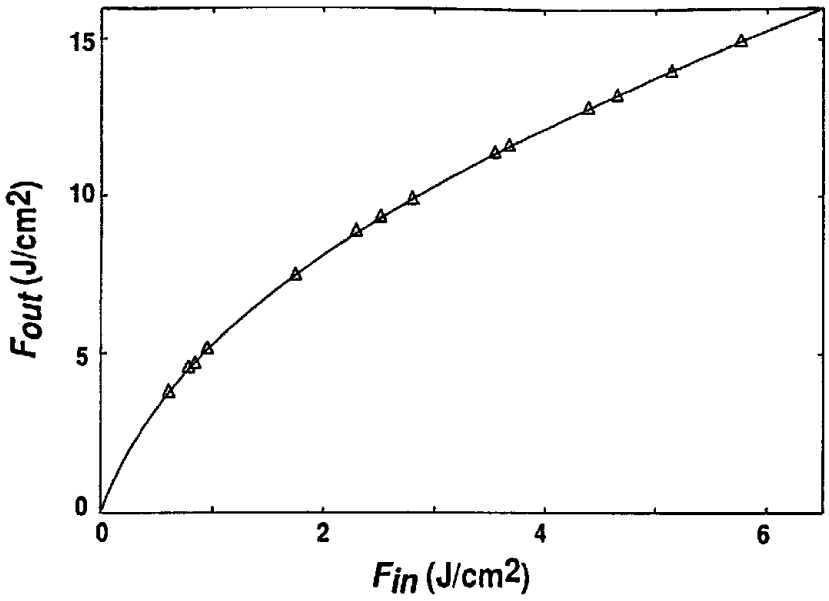

x

Fig. 7: The 2-ion model accurately fits both high and low fluence LG-750 data.

The one and two-ion saturation fluence values for LG-750 were tested in the Nova gain saturation code, using the most recent Nova gain measurements. In the one-ion case, a saturation fluence of 4.3 J/cm^2 at 1 ns is required to produce the correct gain and square pulse distortion. The 20 ns value of 4.52 J/cm^2 measured in both off-line experiments scales to an average saturation fluence of 4.14 J/cm^2 at 1 ns due to lower level lifetime bottlenecking, as determined by previous experiments[17] and modeling[39]. The plot of F_{out} vs F_{in} in Fig 8 shows the pulse length dependence for the Yarema-Milam data. The one-ion saturation fluence value from the OSL experiments predicts the Nova results to within 4%. The two-ion model values obtained from OSL experiments also produce the correct pulse shape to within 4%. The two-ion values obtained from fitting the Yarema-Milam data up to 10 J/cm^2, produce the correct pulse shape to within 8%.

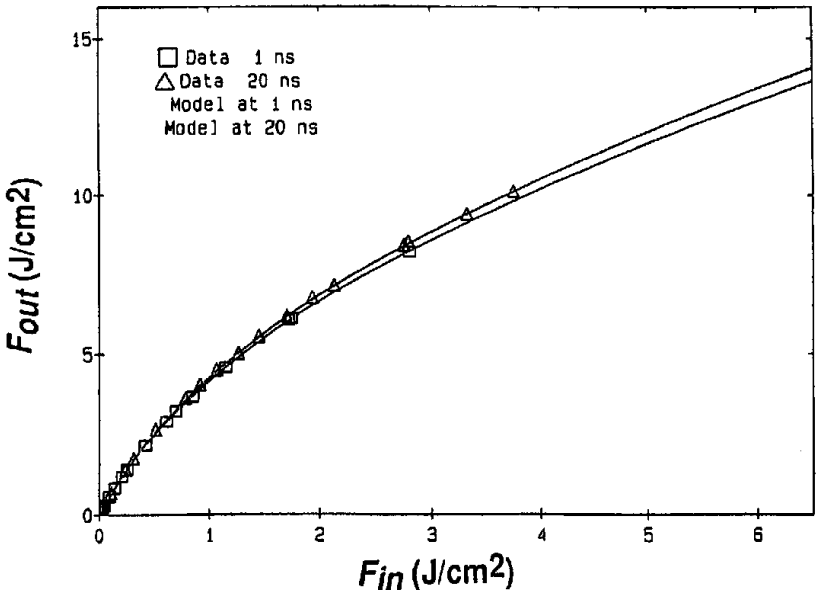

Fig 8: Plot of output fluence vs input fluence shows the pulse length dependence for the Yarema-Milam LG-750 data. The best fit to the data yields a terminal level lifetime of 280 ps.

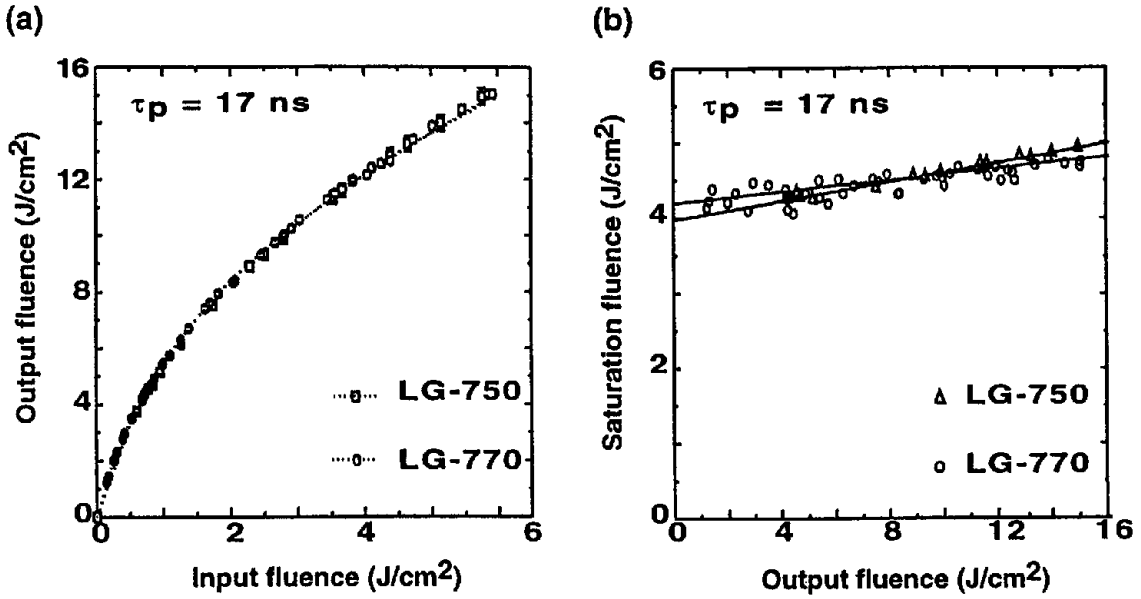

Fig. 9: (a) For long pulse lengths, i.e., pulse length >> terminal level lifetime, gain saturation in LG-770 is comparable to that in LG-750. (b) Plot of saturation fluence vs output fluence shows a slightly steeper slope for LG-750 than LG-770, indicating LG-770 may be slightly more homogeneous than LG-750.

3.1 LG-770

For long pulse lengths, i.e., pulse length >> terminal level lifetime, gain saturation in LG-770 is comparable to that in LG-750, as shown in Fig. 9(a). The single-ion model predicts an average saturation fluence of 4.71 J/cm^2 (σ_{sat} = 0.05 J/cm^2, $\sigma_{residual}$ = 0.18 J/cm^2) for LG-750 and 4.63 J/cm^2 (σ_{sat} = 0.01 J/cm^2, $\sigma_{residual}$ = 0.11 J/cm^2) for LG-770. The plot of F_{sat} vs F_{out} in Fig. 9(b) shows a slightly steeper slope for LG-750 than LG-770, indicating LG-770 may be more homogeneous than LG-750. The extraction data for LG-770 at 1, 5, and 17 ns was modeled using the time-dependent two-ion model described by Eqn. (5), and the results are shown in Fig. 10. The 1 ns and 20 ns Yarema-Milam data were also modeled (Fig. 8). The most significant difference between the LG-770 and LG-750 parameters is the terminal level lifetime required to fit the data. A terminal level lifetime of ~ 1.7 ns is required to fit the data from all three pulse lengths. This value can be reduced to ~ 0.43 ns by eliminating the 5 ns data, which has a larger amount of scatter than the other data sets and could erroneously influence the fitting routine. It should be noted that there were no experimental irregularities in the 5 ns experiments to account for this scatter, however, this does provide a lower bound for the lower level lifetime. The longer terminal level lifetime in LG-770 could cause a reduction in extraction efficiency for short pulse lengths. However, this effect is somewhat mitigated by the fact that LG-770 has a higher cross-section than LG-750. The extraction efficiency vs input fluence for LG-750 and LG-770 is plotted in Fig. 11. A summary of the calculated parameters for LG-750 and LG-770 is given in Table 2.

The long terminal level lifetime in LG-770 is unexpected as measurements of similar Nd:doped phosphate glasses have predicted terminal level lifetimes that are less than 300 ps.[48] However, the terminal level lifetime can be affected by the composition of the glass. The terminal level lifetimes of four Nd:doped phosphate glasses and one Nd:doped crystal are given in Table 2, along with the partial compositions of the glasses.[48] The terminal level lifetime tends to decrease as lighter compounds replace heavier ones in the glass composition. While this does not appear to apply in the case of LG-770, it is possible that the composition of the glass, which is currently proprietary, is sufficiently different

from the glasses measured to date to cause a longer lower level lifetime. It has also been shown experimentally and from multiphonon theory, that higher phonon frequencies lead to shorter nonradiative lifetimes.[52] Further experiments are required to reduce the uncertainty of the lower level lifetime in LG-770. In particular, a measurement of the emission spectrum could provide valuable information on the phonon spectrum of LG-770, which could explain the variation in the lifetime.

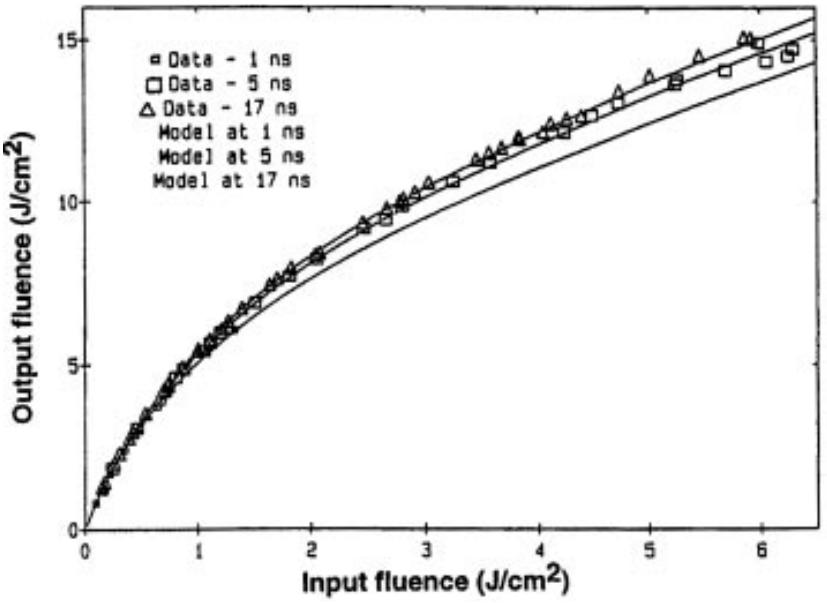

Fig. 10: The extraction data for LG-770 at 1, 5, and 17 ns was modeled using the time-dependent two-ion model described by Eqn. (5).

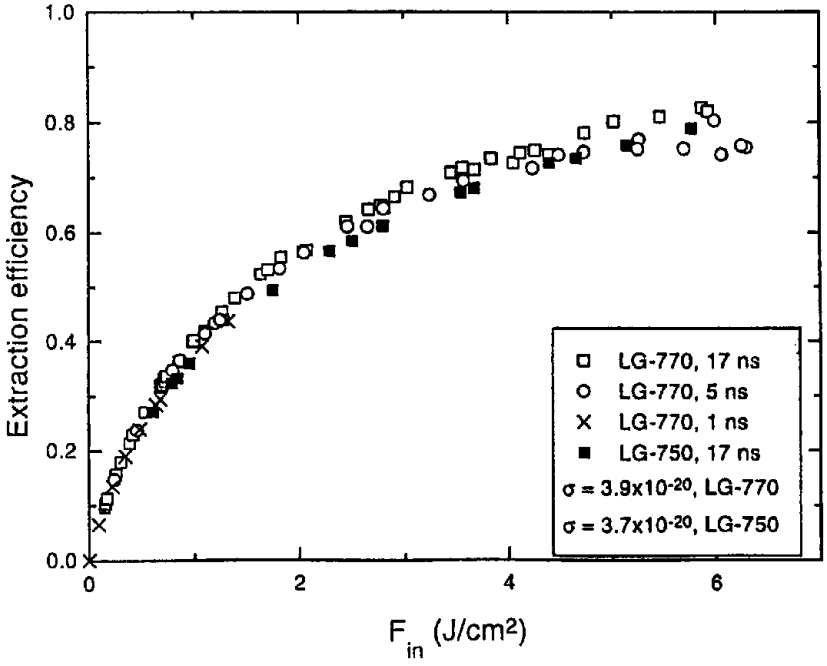

Fig. 11: Extraction efficiency vs input fluence for LG-750 and LG-770.

TABLE 2

Glass Name	Composition	Terminal level lifetime (ps)
LG-750	proprietary phosphate glass	253
FOM-137	proprietary phosphate glass	250
APG-1	proprietary phosphate glass	192
APG-124	proprietary phosphate glass	200
APG-2	proprietary phosphate glass	158
CFAP (crystal)	Ca5(PO4)5F crystal	156

4.0 SUMMARY

We have reproduced previous saturation data in LG-750 and extended the data to output fluences up to 15 J/cm^2. The data has been successfully modeled with both one and two-ion saturation fluence models, and is consistent with previous results at low fluence. The data indicates that the saturation fluence increases linearly as a function of output fluence, requiring a higher saturation fluence than expected to accurately model the data for high output fluence. This is consistent with the fact that the cross-section is an ensemble average, thus a different group of ions may be extracted at high fluence. For long pulse lengths, i.e., pulse length >> terminal level lifetime, gain saturation in LG-770 is comparable to that in LG-750. LG-770 appears to have a longer terminal level lifetime than LG-750, which affects extraction efficiency for short pulse lengths. This effect is somewhat mitigated by the higher cross-section value in LG-770.

5.0 ACKNOWLEDGEMENTS

The authors would like to thank C. Bibeau and J. Trenholme for many helpful discussions, and P. Danforth and W. Sell for their assistance in collecting the data. This work was performed under the auspices of the U.S. Department of Energy by the Lawrence Livermore National Laboratory under Contract No. W-7405-ENG-48.

6.0 REFERENCES

[1] L. M. Frantz and J. S. Nodvik, *J. Appl. Phys.*, **34**, pp. 2346-2349, 1963.
[2] E. Snitzer and C. G. Young, in *Lasers*, New York: Marcel Dekker, Inc., 1968, pp. 191-256.
[3] W. Koechner, *Solid-State Laser Engineering*. New York, NY: Springer-Verlag, 1976.
[4] G. J. Linford, R. A. Saroyan, J. B. Trenholme, and M. J. Weber, **QE-15**, pp. 510-523, 1979.
[5] J. L. Emmett, W. F. Krupke, and J. B. Trenholme, *Sov. J. Quantum Electron.*, **13**, pp. 1-23,1983.
[6] A. E. Siegman, *Lasers*. Mill Valley, CA: University Science Books, 1986.
[7] J. M. Pellegrino, W. M. Yen, and M. J. Weber, *J. Appl. Phys.*, **51**, pp. 6332-6336, 1980.
[8] C. Brecher, L. A. Riseberg, and M. J. Weber, *Phys. Rev. B*, **18**, pp. 5799-5811, 1978.
[9] T. T. Basiev, A.Yu.Dergachev, E. O. Kirpichenkova, Y. V. Orlovskii, and V. V. Osiko, *Sov.J. Quantum Electron.*, **17**, pp. 1289-1291, 1987.
[10] S. A. Brawer and M. J. Weber, *Appl. Phys. Lett.*, **35**, pp. 31-33, 1979.
[11] J. A. Caird, A. J. Ramponi, and P. R. Staver, *J. Opt. Soc. Am. B*, **8**, pp. 1391-1403, 1991.
[12] T. T. Basiev, A. Y. Dergachev, Y. V. Orlovski, S. Georgeschu, and A. Lupei, *Digest of the Topical Meeting on Tunable Solid State Lasers, North Falmouth, MA*, 1989.
[13] D. W. Hall, *Ph.D. Thesis, University of California, Davis*, 1982.
[14] D. W. Hall and M. J. Weber, *Appl. Phys. Lett.*, **42**, pp. 157-159, 1983.
[15] D. W. Hall, M. J. Weber, and R. T. Brundage, *J. Appl. Phys*., **55**, 1984.
[16] B. K. Sinha and S. R. Kumbhare, *Opt. Comm.*, **73**, pp. 239-243, 1989.
[17] S. M. Yarema and D. Milam, *IEEE J. Quantum Electron.*, **QE-18**, pp. 1941-1946, 1982.

[18] W. E. Martin, D. Milam, and J. B. Trenholme, *Laser Program Annual Report-79*, vol. UCRL-50021-79. Livermore, CA, 1980, pp. 2.160-2.170.
[19] W. F. Hagen, *Laser Program Annual Report-1983*, vol. UCRL-500021-83. Livermore, CA, 1984, pp. 6.48-6.56.
[20] V. V. Ivanov, Y. V. Senatskii, and G. V. Sklizkov, *Sov. J. Quantum Electron.*, **17**, pp. 184-191, 1987.
[21] V. I. Nikitin, M. S. Soskin, and A. I. Khizhnyak, *Sov. Tech. Phys. Lett.*, **2**, pp. 64-66, 1976.
[22] L. E. Ageeva and N. B. Brachovskaya, *Sov. J. Quantum Electron.*, **7**, pp. 1379-1382, 1977.
[23] W. E. Martin and D. Milam, *Appl. Phys. Lett.*, **32**, pp. 816-818, 1978.
[24] D. Milam, *IEEE J. Quantum Electron.*, **QE-19**, pp. 1217, 1983.
[25] W. E. Martin and D. Milam, *IEEE J. Quantum Electron.*, **QE-18**, pp. 1155-1163, 1982.
[26] V. I. Kryzhanovskii, V. A. Serebryakov, and V. E. Yashin, *Sov. J. Quantum Electron.*, **17**, pp. 1531-1535, 1987.
[27] V. N. Alekseev, D. I. Dmitriev, A. N. Zhilin, and V. N. Chernov, *Sov. J. Quantum Electron.*, **15**, pp. 95-97, 1985.
[28] M. E. Brodov, I. V. Epatko, A. V. Ivanov, P. P. Pashinin, and R. V. Serov, *Sov. J. Quantum Electron.*, **17**, pp. 1528-1531, 1987.
[29] B. S. Guba, A. A. Mak, S. L. Potapov, B. M. Sedov, and V. V. Shashkin, *Sov. J. Quantum Electron.*, **12**, pp. 772-775, 1982.
[30] D. W. Hall, R. A. Haas, W. F. Krupke, and M. J. Weber, *IEEE J. Quantum Electron.*, **QE-19**, pp. 1704-1717, 1983.
[31] D. W. Hall and M. J. Weber, *IEEE J. Quantum Electron.*, **QE-20**, pp. 831-834, 1984.
[32] D. W. Hall, W. F. Hagen, and M. J. Weber, *IEEE J. Quantum Electron.*, **QE-22**, pp. 793-796, 1986.
[33] V. V. Ivanov, Y. V. Senatskii, and G. V. Sklizkov, *Sov. J. Quantum Electron.*, **19**, pp. 1106-1108, 1989.
[34] B. S. Guba and V. V. Lyubimov, *Sov. J. Quantum Electron.*, **20**, pp. 1075-1078, 1990.
[35] E. V. Eshmemet'eva, V. I. Korolev, E. P. Mesnyankin, V. A. Serebryakov, V. V. Shashkin, and V. E. Yashin, *Sov. J. Quantum Electron.*, **22**, pp. 775-778, 1992.
[36] A. A. Mak, B. G. Malinin, V. A. Novikov, D. S. Prilezhaev, A. I. Stepanov, and V. I. Ustyugov, *Sov. Tech. Phys.*, **14**, pp. 1418, 1970.
[37] K. V. Gratsianov, B. S. Guba, B. G. Malinin, D. S. Prilezhaev, O. B. Raba, B. M. Sedov, and A. I. Stepanov, *Opt. Spectrosc. (USSR)*, **51**, pp. 88, 1981.
[38] A. E. Danilov, V. V. Orlov, S. M. Savchenko, A. F. Suchkov, S. I. Fedotov, and A. L. Khitrov, *Sov. J. Quantum Electron.*, **15**, pp. 139-140, 1985.
[39] C. Bibeau, J. B. Trenholme, and S. A. Payne, *IEEE J. Quantum Electron.*, **32**, pp. 1487-1496, 1996.
[40] V. V. Ivanov, Y. V. Senatskii, and G. V. Sklizkov, *Sov. J. Quantum Electron.*, **16**, pp. 422-424, 1986.
[41] L. W. Casperson and A. Yariv, *IEEE J. Quantum Electron.*, **QE-8**, pp. 80-85, 1972.
[42] A. C. Erlandson, G. F. Albrecht, and S. E. Stokowski, *J. Opt. Soc. Am. B*, **9**, pp. 214-222, 1992.
[43] K. N. Seeber, *IEEE Trans. Electron. Devices*, **ED-12**, pp. 63-66, 1965.
[44] A. Y. Cabezas and R. P. Treat, *J. Appl. Phys.*, **37**, pp. 3556-3563, 1966.
[45] A. Y. Cabezas, G. L. McAllister, and W. K. Ng, *J. Appl. Phys.*, **38**, pp. 3487-3491, 1967.
[46] P. V. Avizonis and R. L. Grotbeck, *J. Appl. Phys.*, **37**, pp. 687-693, 1966.
[47] J. B. Trenholme and E. J. Goodwin, *Laser Program Annual Report-1977*, vol. UCRL-50021-77. Livermore, CA, 1978, pp. 2.236-2.238.
[48] C. Bibeau, S. A. Payne, and H. T. Powell, *J. Opt. Soc. Am. B*, **12**, pp. 1981-1992, 1995.
[49] P. R. Bevington, *Data reduction and error analysis for the physical sciences*. New York: McGraw-Hill Book Co., 1969.
[50] J. Campbell, *internal memo*, UCRL-JC-124244.
[51] B. V. Wonterghem, *personal communication*, 1994.
[52] C. B. Layne, W. H. Lowdermilk, and M. J. Weber, *Phys. Rev. B*, vol. 16, pp. 10-20, 1977.